Localized Surface Plasmon Resonance in Free Silver Nanoclusters Ag n , n = 20–147

Romain Schira, Franck Rabilloud

Localized Surface Plasmon Resonance in Free Silver Nanoclusters Ag_n, $n = 20 - 147$

Romain Schira and Franck Rabilloud*

Institut Lumière Matière, UMR5306 Université Claude Bernard Lyon 1 - CNRS, Université de Lyon 69622 Villeurbanne Cedex, France

E-mail: franck.rabilloud@univ-lyon1.fr

*To whom correspondence should be addressed

Abstract

Absorption spectra of silver nanoclusters, Ag_n with $n = 20-147$, are investigated in the framework of the time-dependent density functional theory (TDDFT) with the use of a range-separated hybrid density functional. Our calculated spectra reproduce well the experimental data. The plasmon-like band energy is situated at about 4 eV for all clusters in gas phase. A description of the plasmonic behavior is given using analyses and tools derived from *ab initio* quantum calculations. The plasmon band originates from multiple peaks gathered in a relatively small range of energy. High intensive peaks near the center of the band present a strong plasmonic character which has been characterized in terms of transition density, hole-electron excitation, transition contribution map (TCM), and generalized plasmonicity index (GPI).

Introduction

Metal nanoparticles have received much attention in recent years in both science and technology due to their unique optical, electronic and catalytic properties.[1] Notably, the collective excitation of conduction electrons and their interaction with a electromagnetic field give raise to the so called localized surface-plasmon resonance (LSPR), and cause a giant absorption band in the UV-visible domain. Plasmonics makes metal nanoparticles very interesting for a range of applications such as biological sensing,[2] cancer therapy,[3,4] optoelectronic devices,[5,6] photocatalysis,[7] photovoltaics,[8,9] surface-enhanced Raman spectroscopy (SERS),[10,11] etc. The LSPR frequency can be tuned through the shape, size and composition of the nanoparticle[12–14] but is also dependent of the environment.[15] The plasmon band originates from multiple peaks gathered in a small range of frequencies. The collective modes are envelopes of coherent superpositions of electron-hole excitations.[16–18] But at small size, the plasmon band of noble metal generally disappears i.e. the collective effect of the electron excitation is reduced, because of the discreteness of electronic states, the band is fragmented into discrete peaks which are scattered in a large range of frequencies. Then they are likely to be lost

in the interbands (transitions associated to d-electrons)[19] or in the bands resulting from hybridization with protecting ligands bound to the surface of clusters.[20,21] But silver is a exception since the plasmon-like band is clearly visible down to small size bare clusters of about 18-20 atoms[22,23] thanks to a relatively strong alkali-like character with a large s-d separation.[24]

Absorption spectra of medium-sized and small-sized silver clusters have been measured in vacuum,[25] in solution,[26] in solid rare-gas matrices,[22,27–29] and in supported samples on glass.[30] Very recently, spectra of Ag_n clusters ($n = 5 - 120$) have been published,[23] they show a plasmon band situated between 3.9 and 4.1 eV in vacuum, with variation with cluster size according to the spherical electronic shell model. Also, the plasmon energy is strongly blue shifted with the decreasing cluster size since it is likely to be close to 3.2 eV for large nanoparticles.[13]

Theoretically, the description of the optical properties of large noble metal nanoparticles have been intensively and successfully investigated using classical optics by solving the Maxwell's equations for electromagnetic waves interacting with particles characterized by the dielectric function of the bulk, eventually coupled with a hydrodynamic model,[31] or with more sophisticated semiclassical methods able to describe the core polarization and its effect on the optical response like the random phase approximation (RPA),[32,33] or approaches based on time-dependent local density approximation and jellium models.[34,35] In these semiclassical calculations, the plasmon resonance reflects a collective excitation of the s valence electrons, but the effects of the d-electrons are only accounted for by using the bulk dielectric function and the atomic structure is neglected. Investigating small nanoclusters of some tens of atoms requires a fully quantum treatment for all electrons. Such calculations are now possible in the framework of the Time-Dependent Density Functional Theory (TDDFT).[36] Recently, a few TDDFT studies have been performed on Ag_n clusters with $n \sim 8 - 300$ atoms.[22,24,37–45] However, while most studies used a local or semi-local formulation for the exchange and correlation functional, one of us have shown that the use of a hybrid functional is required

to correctly describe the excitations of d-type electrons which present charge-transfer and Rydberg characters.[46,47] Such excitations cannot be described within TDDFT with a local or semi-local density functional in the adiabatic approximation used in standard calculations.[48] The $d \rightarrow sp$ excitation energies are significantly underestimated at TDDFT/GGA level and consequently the interband transitions lead to a large band close to 3 eV which is often confused, or mixed, with the $sp \rightarrow sp$ intrabands. For silver clusters, the description of excited states within the adiabatic approximation in standard TDDFT calculations requires a correction of the self-interaction error (SIE) and a correct asymptotic behavior. The best results have been obtained with range separated hybrid functionals (RSHs) which resolve a significant part of the SIE problems and also improve the asymptotic behavior at long range thanks to the inclusion of the Hartree-Fock exchange.[46,47] But the cost of calculations becomes heavier.

In a very recent paper[23], our colleagues have furnished the experimental absorption spectra of Ag_n clusters ($n = 5-120$) embedded in a weakly interacting neon matrix, and we have given some TDDFT/RSH calculations of Ag_n@Neon in which both silver and neon atoms were explicitly treated. Our calculated spectra were found in excellent agreement with the experimental ones, suggesting that our simulation methodology is correct. In the present paper, we give the absorption spectra of free Ag_n, $n = 20 - 92$, and Ag_{147}^+ nanoclusters calculated within the TDDFT approach with a RSH-type functional, and we furnish a description of the plasmonic behavior using analyses and tools derived from *ab initio* quantum calculations.

Theoretical Method

Absorption spectra have been calculated in the framework of the Time-Dependent Density Functional Theory (TDDFT) using the range-separated hybrid (RSH) density functional ωB97x[49] which includes an increasing part of exact Hartree-Fock exchange at long range

(from 16% at short range to 100% at long range). Calculations treat the 19 valence electrons per silver atom within a relativistic effective core potential (RECP) together with the corresponding Gaussian basis set.[50]

The geometrical structures were taken from a study by Chen et al[51] dedicated to the prediction of structures of silver clusters using a genetic algorithm with an embedded atom method potential, except the structure of Ag_{20} which is the ground state structure of C_s symmetry optimized at DFT level in Ref.[22] Geometrical structures were relaxed with ωB97x before calculating the absorption spectra (Fig. S1 in Supporting Information). Of course we cannot be sure that a more stable cluster than those considered in our calculations does not exist. But the absorption spectra calculated with several isomers of Ag_{20} and Ag_{42} (Fig. S2 and S3 in Supporting information) show that the spectra characterized by a plasmon-like band are only weakly dependent on the exact geometrical structure as long as the shape is somewhat spherical, as expected for metal clusters with free valence electrons. This is in agreement with a previous work by Durante et al.[52] which has showed that the position of the band energy in gold $Au_{\sim 150}$ clusters is weakly dependent on the shape of the cluster.

The choice of the exchange and correlation density functional was motivated by previous benchmarking works on small clusters[46,47] that we are extending here to larger clusters. In Fig. 1, we compare the performance of three commonly used families of exchange and correlation functionals, namely BP86[53,54] which is a standard GGA (Generalised Gradient Approximation) density functional, the asymptotically corrected (AC-GGA) LB94 potential model [55] which gives a $-1/r$ behavior at long range, and the range-separated hybrid ωB97x. The calculated absorption spectra of Ag_{92}, Ag_{58} and Ag_{55}^{+} are compared to most recent experimental spectra.[23] As expected, only the range-separated hybrid ωB97x is able to reproduce the experimental data. Indeed, TDDFT calculations with a local exchange and correlation potential in the adiabatic approximation can not correctly describe the interband $d \rightarrow sp$ transitions since the latter present Rydberg and long-range charge-transfer characters that can only be described with a RSH-type density functional.[46,47] For the size

$n = 55$, the spectra are calculated for the cation Ag_{55}^{+} (due to the constraints imposed by the ADF Software[56] which can calculate excitation energies only for electronic closed shell systems) while the experimental spectrum is that of the neutral cluster Ag_{55}. That is why the calculated spectrum is blue shifted with respect to the experimental one.

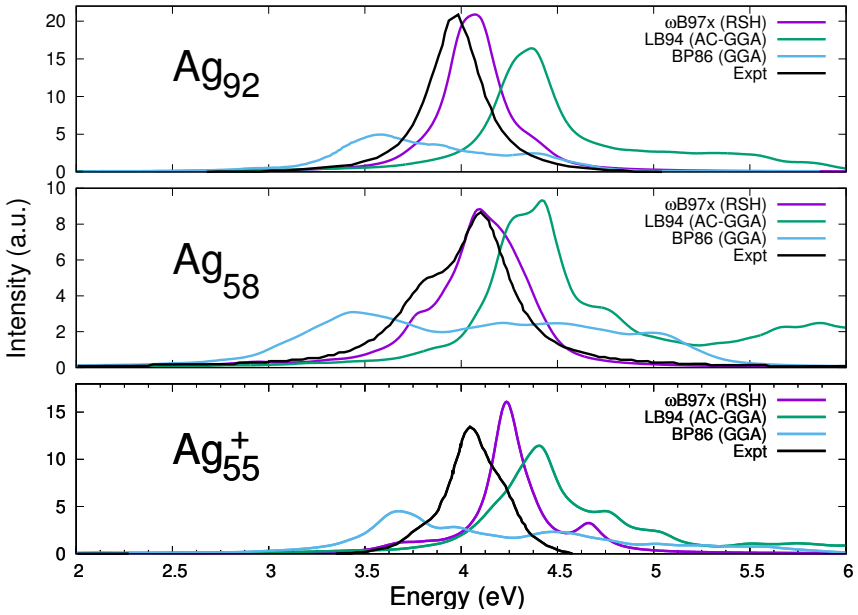

Figure 1: Absorption spectra of silver clusters Ag_n for sizes $n = 92$,58, and 55 calculated with three different families of density-functionals. Experimental data are measured on clusters embedded in a Neon matrix, and are blue-shifted by 0.17 eV to remove the dielectric effects.[23] For the size $n = 55$, the optical response is calculated for the cation while the experimental curve is measured for the neutral species.

All calculations were performed using the program Gaussian09[57] (ωB97x calculations), and the program ADF[56] (LB94 and BP86 calculations). Pre- and postprocessing operations were performed by using the graphical interface Gabedit.[58]

Results and discussion

Absorption spectra

Calculated absorption spectra are given in Fig. 2 together with the experimental ones measured in Neon. The latter have been blue-shifted by 0.17 eV to remove the dielectric matrix

shift as supported by our previous study[23,59] where TDDFT calculations performed in gas phase and in neon matrix have shown that the unique effect of the rare gas matrix is a redshift of the whole spectrum ; this allows to compare the spectra to calculated gas phase values. Let us note that the shift value of 0.17 eV is predicted to have no significant size dependency for $n = 20 - 92$ atoms. The experimental spectrum of Ag_{42} was measured by surface second harmonic generation spectroscopy on size-selected clusters supported on BK7 glass substrate.[30] The calculated absorption spectra showed in Fig. 2 give the oscillator strength as a function of the excitation energy together with a curve obtained by a Lorentz broadening with a full width at half-maximum (fwhm) of 0.08 eV. For all clusters, the peaks with strong oscillator strengths are in the 3.8-4.2 eV range, resulting in an intense band centered at around 4 eV. Both position and shape of experimental spectra are well reproduced. The narrower absorption widths for Ag_{38} (D_{2h}), Ag_{55} (I_h), Ag_{92} (C_{3v}), Ag_{147}^+ (I_h) are due to the high symmetry of the geometrical structure which tends to gather the peaks on a narrow band of energy, while the other clusters are less symmetrical.

For Ag_{20}, the main band is centered at 4 eV and composed of four strong peaks in the 3.97-4.04 eV range. A shoulder at 3.72 eV is also visible. For Ag_{35}, the spectrum shows a relative wide band, composed of two peaks at 3.95 and 4.12 eV, respectively. The first peak is mainly due to two excitations at 3.91 and 3.96 eV respectively, while the second one is due to several less intense transitions in the 4.11-4.18 eV range. The calculated spectrum fits well the experimental spectrum that also shows two peaks. For Ag_{42}, the spectrum consists of a large band due to a range of peaks spanning the 3.7-4.5 eV energy range. The experimental spectrum in Neon is not available, but Lünskens et al.[30] have measured the band plasmon by surface second harmonic generation spectroscopy on clusters supported on BK7 glass substrate. Their spectrum is reproduced in Fig. 2 with a band centered at 3.78 eV. The red-shifted by about 0.15 eV compared to our calculated data in gas phase is likely due to dielectric effects of the oxide substrate. Fig. S2, in ESI, gives the spectra calculated with two different isomers, predicted to be the ground state using energetic models based on atomistic

potentials.[51,60] Both spectra are found to be very similar, which confirms that the optical response of metal clusters is only weakly dependent on the exact geometrical structure as long as the shape is somewhat spherical. For Ag_{55}, the plasmon band is centered at 4.11 eV, slightly blueshifted with respect to the experimental band at 4.07 eV. A secondary band centered at 4.56 eV is also calculated, but not see in experiments.[23] Interestingly both bands were calculated at 4.23 and 4.66 eV respectively for the cation Ag_{55}^+ (Fig. 1). The calculated spectrum of Ag_{58} shows a main transition at 4.08 eV and a less intense one at 3.77 eV, in excellent agreement with the experimental data showing these features at 4.11 and 3.81 eV[23]. The spectrum of Ag_{84} shows a wide band due to a range of peaks spanning the 3.7-4.5 eV energy range, with a maximum at 4.01 eV, and two shoulders at 3.91 eV and 4.32 eV respectively. The C_{3v} symmetry of Ag_{92} leads to a relatively narrow absorption band, it is centered at 4.05 eV, slightly blue-shifted compared to the experimental value of 3.97 eV[23]. Finally, we give the absorption spectrum of the cation Ag_{147}^+ with a I_h geometrical structure (calculation is less cumbersome for the cation than it is for the neutral cluster, thanks to an even number of electrons). The giant band with a narrow width of around 0.2 eV at full width at half maximum (FWHM),is centered at 4.22 eV, and composed of three main transitions at 4.22 and 4.25 eV. Following the shift of 0.12 eV between spectra of Ag_{55}^+ and Ag_{55} (see above), the absorption band of neutral Ag_{147} is likely to be redshifted to about 4 or 4.1 eV.

Overall, our calculated spectra obtained with cumbersome calculations (TDDFT/RSH with more 3200 primitive gaussians is time-consuming) reproduce well the experimental ones.

Analysis of excitations

To characterize the plasmonic excitation, we first furnish some visual interpretations. In the adiabatic linear-response formalism of the TDDFT, the transition density associated to a single excited state is typically expanded in the product of occupied and virtual Kohn-Sham

molecular orbitals:

$$T(\vec{r}) = \sum_{i \to s} F_{i,s}\phi_i(\vec{r})\phi_s^*(\vec{r}) + \sum_{i \leftarrow s} F_{s,i}\phi_i^*(\vec{r})\phi_s(\vec{r}), \quad (1)$$

where i and s label the occupied and virtual orbitals respectively, and $F_{i,s}$ is the component of the TDDFT eigenvector, which is composed of occupied-unoccupied $i \to s$ excitations and $i \leftarrow s$ desexcitations. As a matter of fact, in the current formalism the transition density is equivalent to the induced density defined by the Fourier transform of the difference between the charge density evolving after a perturbation and the ground state density $FT(\rho(\vec{r},t) - \rho_0(\vec{r}))$. Isosurface plots of the transition density for some intense peaks in the absorption spectra of Ag_{20}, Ag_{92} and Ag_{147}^+ are showed in Fig. 3. As explained above, the plasmon band originates from multiple peaks gathered in a small range of energy, and can be seen as an envelope of coherent excitations represented by the lorentzian curve in Fig. 2. The excitations considered in Fig. 3 are those with highest oscillator strengths and are located at the center of the band (near 4 eV). The transition densities display a typical dipolar shape, which represent the oscillation of the electron density along one direction, which could be expected to be, for instance, that of the electric field of a laser. The density change affects many two opposing sides of the cluster, with strong contribution from s electrons, while less intense contributions from d electrons polarize in the opposite direction and thus create a countering screening field. The collective behavior is visible even for the small cluster Ag_{20}. All plots correspond to the classical picture of LSPRs as a charge cloud oscillating between the opposite sides of the cluster.

We can also furnish a representation in terms of electron-hole pair where an electron leaves the hole domain and goes to electron domain during the excitation. The "hole" and the "electron" can be defined in different ways. In previous studies,[47,61] we gave the electron density difference between the excited and ground states for some of the main peaks of Ag_{20} clusters. Here we adopt the definition of hole and electron proposed by T. Lu and C. Zhong

in Multiwfn program.[62] The density distribution of hole and electron is defined as:

$$\begin{aligned}
\rho^{hole}(\vec{r}) &= \rho^{hole}_{local}(\vec{r}) + \rho^{hole}_{cross}(\vec{r}), \qquad (2)\\
&= \sum_{i\to s} \left(F_{i,s}\right)^2 \phi_i(\vec{r})\phi_i(\vec{r}) - \sum_{i\leftarrow s} \left(F_{i,s}\right)^2 \phi_i(\vec{r})\phi_i(\vec{r})\\
&+ \sum_{i\to s}\sum_{j\neq i\to s} F_{i,s}F_{j,s}\phi_i(\vec{r})\phi_j(\vec{r}) - \sum_{i\leftarrow s}\sum_{j\neq i\leftarrow s} F_{i,s}F_{j,s}\phi_i(\vec{r})\phi_j(\vec{r}),\\
\rho^{elec}(\vec{r}) &= \rho^{elec}_{local}(\vec{r}) + \rho^{elec}_{cross}(\vec{r}), \qquad (3)\\
&= \sum_{i\to s} \left(F_{i,s}\right)^2 \phi_s(\vec{r})\phi_s(\vec{r}) - \sum_{i\leftarrow s} \left(F_{i,s}\right)^2 \phi_s(\vec{r})\phi_s(\vec{r})\\
&+ \sum_{i\to s}\sum_{i\to u\neq s} F_{i,s}F_{i,u}\phi_s(\vec{r})\phi_u(\vec{r}) - \sum_{i\leftarrow s}\sum_{i\leftarrow u\neq s} F_{i,s}F_{i,u}\phi_s(\vec{r})\phi_u(\vec{r}).
\end{aligned}$$

The terms "local" and "cross" stand for the contribution of local term and cross term to the hole and electron distribution, respectively. Both ρ^{hole} and ρ^{elec} integrate to one over all space. The charge density difference between excited state and ground state is then evaluated as

$$\Delta\rho(\vec{r}) = \rho^{elec}(\vec{r}) - \rho^{hole}(\vec{r}). \qquad (4)$$

Isovalue plots of $\Delta\rho(\vec{r})$ for some intense peaks are given in Fig. 4. Red colored regions correspond to depletion of the electron density during the transition, while blue regions correspond to an increase of the electron density. In the case of Ag_{92} and Ag^{+}_{147}, plots show clearly that during the transition the electron is transferred from the core to the surface of the cluster. Actually, the hole density is distributed over both the core and the surface of the cluster while the electron density is mainly located on the surface of the cluster. For Ag_{20}, there is only one atom in the core, and then the hole is partially localized on the surface. Consequently, the transfer from the core to the surface is less pronounced.

Change densities are mainly associated to s and p orbitals, with very few d contributions. In a previous works,[47] the d character in the plasmonic excitation was evaluated to about 10%, which seems to be in agreement with the classical picture of the plasmon likely to be associated to excitations of s electrons, with a few contribution of d electrons.

Following previous works,[19,42,63] we also furnish an analysis of the electron transitions based on transition contribution map (TCM) plots. In the TDDFT approach, each excited states can be described by a sum of monoexcitations and desexcitations with a relative contribution $F_{i,s}$ (See equation 1). In the TCM plot associated to a given excited state, each monoexcitation is represented by one point in a map where the axis are the eigenvalue of the initial state ξ_i and the eigenvalue of the final state ξ_s, while the magnitude of each transition is broadened by Gaussians (with a smoothing parameter σ):

$$M_{TCM}(\xi_o, \xi_v) = \sum_{i,s} \frac{|F_{i,s}|}{\sigma^2 2\pi} e^{\frac{(\xi_o-\xi_i)^2+(\xi_v-\xi_s)^2}{2\sigma^2}}. \quad (5)$$

TCM plots reveal the energies of the initial and final orbitals of the main transitions involved in an excited state. Fig. 5 shows the TCM maps in the case of Ag_{92} together with the density of state (DOS). The *sp* band covers all occupied and virtual orbitals closed to the Fermi level, while the *d* orbitals are confined in a band with an upper limit at about 4.7 eV below the Fermi level. The HOMO-LUMO gap is calculated to be 3 eV because of the use of an hybrid functional which shifts upward the energies of unoccupied orbitals. This leads to get much better excitation energies. All intense spots in the TCM plots for Ag_{92} correspond to intraband $sp \rightarrow sp$ configurations, as expected for plasmonic excitations. In Fig. 5, we show TCM plots for two representative transitions. One is a strong transition (label (a)) at 3.98 eV, near the center of the plasmon, while the other (b), much less intense, is located at 4.35 eV. The maps reflect that the excited state (a) has a stronger plasmonic character than the transition (b). Indeed, the excited state (b) is due to monoexcitations located in a narrowed diagonal band with a few intense spots (in red) placed on a line corresponding to $\xi_i - \xi_s = \Delta$, where Δ is a constant. In contrast, the excitation (a) is made of many intense spots (in red) distributed on a large domain of $\xi_i - \xi_s$ values. The collective nature of the plasmon can be inferred by the presence of many spots with strong contributions in the TCM. Some desexcitations implying *sp* orbitals are also visible for the transition (a). The

TCM maps for three transitions in Ag_{20} is plotted in Fig. 6. Two transitions, labelled (b) and (c), located near the center of the plasmon-like band present a strong plasmon character with several intense spots distributed in a large domain of energy. In contrast, the state situated at 3.69 eV is mainly due to a few intense peaks. The interband $d \rightarrow sp$ transitions are more visible than in the case of Ag_{92}.

In conclusion, TCM maps show that the excited states with intense oscillator strengths and placed near the center of the band originate from many monoexcitations distributed on a large domain of energy, while the states placed further away from the center of the plasmon band present a less collective behaviour. However, it is worth noting that all peaks belong to the plasmon. The difference of nature that we noted is the consequence of the fragmentation of the plasmon band that occurs when considering small-sized clusters.

Several studies have tried to classify the electronic excitations in nanostructures, particularly with the aim of characterizing the emergence of plasmons in opposition to single-electron transitions. Plasmon resonances can be distinguished from single-electron transitions since they manifest a strong dependency in electron-electron interaction.[38,44,64] Recently a generalized plasmonicity index (GPI) has been proposed to quantify the plasmonic character of optical excitations.[19,44,65] The electron density change can be evaluated from the Kohn-Sham response function χ_{KS} as

$$\delta\rho(\vec{r},t) = \int \chi_{KS}(\vec{r},\vec{r}',t,t') \left[v_{ext}(\vec{r}',t') + v_{ind}(\vec{r}',t')\right] \mathrm{d}\vec{r}'\mathrm{d}t', \tag{6}$$

where v_{ext} is the external potential applied to the system of interest, and v_{ind} is the induced potential responsible for the external field enhancement, which reads as follows $v_{ind} = v_H + v_{xc}$, the sum of the Hartree and exchange-correlation potentials. GPI is then defined as the quantity[44]

$$\eta = \frac{|\int \delta\rho(\vec{r},\omega) v^*_{ind}(\vec{r},\omega)\mathrm{d}\vec{r}|}{|\int \delta\rho(\vec{r},\omega) v^*_{ext}(\vec{r},\omega)\mathrm{d}\vec{r}|}, \tag{7}$$

where $\delta\rho(\vec{r},\omega)$ is the Fourier transform of $\delta\rho(\vec{r},t)$, and v^*_{ext} and v^*_{ind} denote the complex

conjugate of the corresponding quantities. The index η is a quantitative measure of the interaction between electrons following an external potential, it will be relatively large for plasmonic excitations which produce a large v_{ind}, but much smaller in case of single-electron transitions for which the induced potential remains very low.

For a more practicable use, Zhang et al.[44] have showed that the GPI can be expressed as

$$\eta = \frac{E_{plasmon}}{\Gamma} = \frac{\int \frac{T(\vec{r})T(\vec{r'})}{|\vec{r}-\vec{r'}|} \mathrm{d}\vec{r}\mathrm{d}\vec{r'}}{\Gamma}, \tag{8}$$

where $T(\vec{r})$ is the transition density for the considered excitation. Γ is a broadening parameter coming from the expression of χ_{KS} in the Lehmann representation. As we have no means to express rigorously the damping energy Γ in our TDDFT calculations, and being expected that this term does not contribute to the plasmonic character, we have calculated the $E_{plasmon}$ value as a descriptor for the plasmonic character of a given transition. Transitions with relative large values for $E_{plasmon}$ will present a more pronounced plasmonic character. The term $E_{plasmon}$ is a dimensionless number, and is not normalized. For Ag_{92}, the value of $E_{plasmon}$ is calculated at 0.019 and 0.003 for the transitions (a) and (b) considered in Fig.5, respectively. The factor of 6 between the two values confirms that the excitation (a) is more plasmonic than the exciation (b). For Ag_{20}, the value of $E_{plasmon}$ is 0.013, 0.036, and 0.066 for transitions (a), (b), and (c), respectively, showed in Fig. 6. Therefore the plasmonic character is stronger in the last two transitions than the former. The excitation near the center of the band present a stronger plasmonic character than those located at lower or higher energies.

Conclusions

The optical response of silver clusters have been calculated at TDDFT/RSH level. Overall, the present calculated spectra reproduce well the recently measured experimental spectra. Plasmon band energies are calculated at about 4 eV for all clusters in gas phase. Plasmon

excitations have been characterized in terms of transition density, electron-hole excitation, transition contribution map (TCM), and generalized plasmonicity index (GPI). The plasmon band originates from multiple peaks gathered in a relatively small range of frequencies, and can be seen as an envelope of coherent excitations represented by the lorentzian-type curve for large clusters. High intensive peaks close to the center of the band present a strong plasmonic character described by (i) a transition density which displays a typical dipolar shape that represents the oscillation of the electron density along one direction, (ii) an electron transfer from the core to the surface during the excitation in a electron-hole scheme, (iii) a collective nature which can be inferred by the presence of many spots with strong contributions and distributed on a large domain of energy in the TCM plot, (iv) a relative high value of the GPI. The plasmon band originates from several peaks distributed over a relatively small energy range, all mainly due to intraband $sp \rightarrow sp$ excitations, in agreement with the classical description of the plasmon phenomena as a collective excitation of valence electrons. The present work is one of the first to correctly reproduce the experimental absorption spectra of silver nanoclusters and to describe them with the help of analyses and tools derived from *ab initio* quantum calculations.

Acknowledgement

This work was performed using HPC resources from GENCI-IDRIS (Grant A0030807662) and the Pôle Scientifique de Modélisation Numérique (PSMN). It has received a financial support from the French National Research Agency (Agence Nationale de la Recherche, ANR) in the frame of the project FIT SPRINGS, ANR-14-CE08-0009. The authors gratefully acknowledge J. Lermé for helpful discussions and A.R. Allouche for support for the use of Gabedit.

Supporting Information Available

The supporting information includes the geometrical structures (Figure S1), and the absorption spectra calculated with several isomers of Ag_{20} and Ag_{42} (Figures S2 and S3). This information is available free of charge via the Internet at http://pubs.acs.org.

References

(1) Schwartzberg, A. M.; Zhang, J. Z. Novel Optical Properties and Emerging Applications of Metal Nanostructures. *J. Phys. Chem. C* **2008**, *112*, 10323–10337.

(2) Anker, J. N.; ; Paige-Hall, W.; Lyandres, O.; Shah, N. C.; Zhao, J.; Van-Duyne, R. P. Biosensing with Plasmonic Nanosensors. *Nat. Mater* **2008**, *7*, 442–453.

(3) Gobin, A. M.; Lee, M. H.; Halas, N. J.; James, W. D.; Drezek, R. A.; West, J. L. Near-Infrared Resonant Nanoshells for Combined Optical Imaging and Photothermal Cancer Therapy. *Nano Letters* **2007**, *7*, 1929–1934.

(4) Bardhan, R.; Lal, S.; Joshi, A.; Halas, N. J. Theranostic Nanoshells: From Probe Design to Imaging and Treatment of Cancer. *Acc. Chem. Res.* **2011**, *44*, 936–946.

(5) Aćimović, S. S.; Kreuzer, M. P.; González, M. U.; Quidant, R. Plasmon Near-Field Coupling in Metal Dimers as a Step Toward Single-Molecule Sensing. *ACS Nano* **2009**, *3*, 1231–1237.

(6) Chen, Y.-S.; Choi, H.; Kamat, P. V. Metal-Cluster-Sensitized Solar Cells. A New Class of Thiolated Gold Sensitizers Delivering Efficiency Greater Than 2%. *J. Am. Chem. Soc.* **2013**, *135*, 8822–8825.

(7) Méndez-Medrano, M. G.; Kowalska, E.; Lehoux, A.; Herissan, A.; Ohtani, B.; Bahena, D.; Briois, V.; Colbeau-Justin, C.; Rodriguez-Lopez, J. L. .; Remita, H. Surface Modification of TiO_2 with Ag Nanoparticles and CuO Nanoclusters for Application in Photocatalysis. *J. Phys. Chem. C* **2016**, *120*, 5143–5154.

(8) Atwater, H. A.; Polman, A. Plasmonics for Improved Photovoltaic Devices. *Nature Materials* **2010**, *9*, 205–213.

(9) Knight, M. W.; King, N. S.; Liu, L.; Everitt, H. O.; Nordlander, P.; Halas, N. J. Aluminium for Plasmonics. *ACS Nano* **2014**, *8*, 834–840.

(10) Seney, C. S.; Gutzman, B. M.; Goddard, R. H. Correlation of Size and Surface-Enhanced Raman Scattering Activity of Optical and Spectroscopic Properties for Silver Nanoparticles. *J. Phys. Chem. C* **2009**, *113*, 74–80.

(11) Stamplecoskie, K. G.; Scaiano, J. C.; Tiwari, V. S.; Anis, H. Optimal Size of Silver Nanoparticles for Surface-Enhanced Raman Spectroscopy. *J. Phys. Chem. C* **2011**, *115*, 1403–1409.

(12) Abe, H.; Charlé, K.-P.; Tesche, B.; Schulze, W. Surface Plasmon Absorption of Various Colloidal Metal Particles. *Chem. Phys.* **1982**, *68*, 137–141.

(13) Haberland, H. Looking From Both Sides. *Nature* **2013**, *494*, E1.

(14) Sinha-Roy, R.; Garcia-Gonzalez, P.; Weissker, H.-C.; Rabilloud, F.; Fernandez-Dominguez, A. I. Classical and Ab Initio Plasmonics Meet at Sub-Nanometric Noble Metal Rods. *ACS Photonics* **2017**, *4*, 1484–1493.

(15) Campos, A.; Troc, N.; Cottancin, E.; Pellarin, M.; Weissker, H.-C.; Lermé, J.; Kociak, M.; Hillenkamp, M. Plasmonic Quantum Size Effects in Silver Nanoparticles are Dominated by Interfaces and Local Environments. *Nat. Phys. In press, DOI:10.1038/s41567-018-0345-z* **2018**,

(16) Brack, M. The Physics of Simple Metal Clusters: Self-Consistent Jellium Model and Semiclassical Approaches. *Rev. Mod. Phys.* **1993**, *65*, 677–732.

(17) Xia, C.; Yin, C.; Kresin, V. V. Photoabsorption by Volume Plasmons in Metal Nanoclusters. *Phys. Rev. Lett.* **2009**, *102*, 156802.

(18) Lermé, J. Size Evolution of the Surface Plasmon Resonance Damping in Silver Nanoparticles: Confinement and Dielectric Effects. *J. Phys. Chem. C* **2011**, *115*, 14098–14110.

(19) Malola, S.; Lehtovaara, L.; Enkovaara, J.; Häkkinen, H. Birth of the Localized Surface

Plasmon Resonance in Monolayer-Protected Gold Nanoclusters. *ACS Nano* **2013**, *7*, 10263–10270.

(20) Chakraborty, I.; Erusappan, J.; Govindarajan, A.; Sugi, K. S.; Udayabhaskararao, T.; Ghosh, A.; Pradeep, T. Emergence of Metallicity in Silver Clusters in the 150 Atom Regime: a Study of Differently Sized Silver Clusters. *Nanoscale* **2014**, *6*, 8024–8031.

(21) Bousquet, B.; Cherif, M.; Huang, K.; Rabilloud, F. Absorption Spectra of Aryl Thiol-Coated Silver Nanoclusters: A Time-Dependent Density-Functional Study. *J. Phys. Chem. C* **2015**, *119*, 4268–4277.

(22) Harb, M.; Rabilloud, F.; Simon, D.; Rydlo, A.; Lecoultre, S.; Conus, F.; Rodrigues, V.; Félix, C. Optical Absorption of Small Silver Clusters: Ag_n, (n=422). *J. Chem. Phys.* **2008**, *129*, 194108.

(23) Yu, C.; Schira, R.; Brume, H.; von Issendorff, B.; Rabilloud, F.; Harbich, W. Optical Properties of Size Selected Neutral Ag Clusters: Electronic Shell Structures and the Surface Plasmon Resonance. *Nanoscale* **2018**, *10*, 20821–20827.

(24) Anak, B.; Bencharif, M.; Rabilloud, F. Time-Dependent Density Functional Study of UV-Visible Absorption Spectra of Small Noble Metal Clusters (Cu_n, Ag_n, Au_n, n = 29, 20). *RSC Adv.* **2014**, *4*, 13001–13011.

(25) Tiggesbäumker, J.; Köller, L.; Meiwes-Broer, K.-H.; Liebsch, A. Blue Shift of the Mie Plasma Frequency in Ag Clusters and Particles. *Phys. Rev. A* **1993**, *48*, 1749–1752.

(26) Bakr, O. M.; Amendola, V.; Aikens, C. M.; Wenseleers, W.; Li, R.; Negro, L. D.; Schatz, C.; Stellacci, F. Silver Nanoparticles with Broad Multiband Linear Optical Absorption. *Angew. Chem. Int. Ed.* **2009**, *48*, 5921–5926.

(27) Fedrigo, S.; Harbich, W.; Buttet, J. Collective Dipole Oscillations in Small Silver Clusters Embedded in Rare-Gas Matrices. *Phys. Rev. B* **1993**, *47*, 10706–10715.

(28) Harbich, W.; Fedrigo, S.; J.Buttet, The Optical Absorption Spectra of Small Silver Clusters (n=8–39) Embedded in Rare Gas Matrices. *Zeitschrift für Physik D Atoms, Molecules and Clusters* **1993**, *26*, 138–140.

(29) Lecoultre, S.; Rydlo, A.; Buttet, J.; Félix, C.; Gilb, S.; Harbich., W. Ultraviolet-Visible Absorption of Small Silver Clusters in Neon: Ag_n (n = 19). *J. Chem. Phys.* **2011**, *134*, 184504.

(30) Lünskens, T.; Heister, P.; Walenta, M. T. C. A.; Kartouzian, A.; Heiz, U. Plasmons in Supported Size-Selected Silver Nanoclusters. *Phys. Chem. Chem. Phys.* **2015**, *17*, 17541–17544.

(31) Christensen, T.; Yan, W.; Raza, S.; Jauho, A.-P.; Mortensen, N. A.; Wubs, M. Nonlocal Response of Metallic Nanospheres Probed by Light, Electrons, and Atoms. *ACS Nano* **2014**, *8*, 1745–1758.

(32) Kresin, V. V. Collective Resonances in Silver Clusters: Role of d Electrons and the Polarization-Free Surface Layer. *Phys. Rev. B* **1993**, *51*, 1844.

(33) Xuan, F.; Guet, C. Core-Polarization-Corrected Random-Phase Approximation with Exact Exchange for Dipole Surface Plasmons in Silver Clusters. *Phys. Rev. A* **2016**, *94*, 043415.

(34) Serra, L.; Rubio, A. Core Polarization in the Optical Response of Metal Clusters: Generalized Time-Dependent Density-Functional Theory. *Phys. Rev. Lett.* **1997**, *78*, 1428.

(35) Lermé, J. Introduction of Quantum Finite-Size Effects in the Mie's Theory for a Multilayered Metal Sphere in the Dipolar Approximation: Application to Free and Matrix-Embedded Noble Metal Clusters. *Eur. Phys. J. D* **2000**, *10*, 265–277.

(36) Casida, M. E. *Recent Advances in Density Functional Methods*; World Scientific, 1995; pp 155–192.

(37) Jensen, L.; Zhao, L. L.; Schatz, G. C. Size-Dependence of the Enhanced Raman Scattering of Pyridine Adsorbed on Ag_n (n = 28, 20) Clusters. *J. Phys. Chem. C* **2007**, *111*, 4756–4764.

(38) Guidez, E. B.; Aikens, C. M. Quantum Mechanical Origin of the Plasmon: From Molecular Systems to Nanoparticles. *2014* **Nanoscale**, *6*, 11512–11527.

(39) Weissker, H.-C.; Lopez-Lozano, X. Surface Plasmons in Quantum-Sized Noble-Metal Clusters: TDDFT Quantum Calculations and the Classical Picture of Charge Oscillations. *Phys. Chem. Chem. Phys.* **2015**, *17*, 28379–28386.

(40) Kuisma, M.; Sakko, A.; Rossi, T.; Larsen, A. H.; Enkovaara, J.; Lehtovaara, L.; Rantala, T. T. Localized Surface Plasmon Resonance in Silver Nanoparticles: Atomistic First-Principles Time-Dependent Density-Functional Theory Calculations. *Phys. Rev. B* **2015**, *91*, 115431.

(41) Titantah, J. T.; Karttunena, M. Ab Initio Calculations of Optical Properties of Silver Clusters: Cross-Over From Molecular to Nanoscale Behavior. *Eur. Phys. J. B* **2016**, *89*, 125.

(42) Baseggio, O.; Vetta, M. D.; Fronzoni, G.; Stener, M.; Sementa, L.; Fortunelli, A.; Calzolar, A. Photoabsorption of Icosahedral Noble Metal Clusters: an Efficient TDDFT Approach to Large-Scale Systems. *J. Phys. Chem. C* **2016**, *120*, 12773–12782.

(43) Koval, P.; Marchesin, F.; Fœrster, D.; Sanchez-Portal, D. Optical Response of Silver Clusters and Their Hollow Shells From Linear-Response TDDFT. *J. Phys. Condens. Matter.* **2016**, *28*, 214001.

(44) Zhang, R.; Bursi, L.; Cox, J. D.; Cui, Y.; Krauter, C. M.; Alabastri, A.; Manjavacas, A.; Calzolari, A.; Corni, S.; Molinari, E. et al. How to Identify Plasmons From the Optical Response of Nanostructures. *ACS Nano* **2017**, *11*, 7321–7335.

(45) Nhat, P. V.; Si, N. T.; Nguyen, M. T. Elucidation of the Molecular and Electronic Structures of Some Magic Silver Clusters Ag_n ($n = 8, 18, 20$). *J. Mol. Model.* **2018**, *24*, 209.

(46) Rabilloud, F. Assessment of the Performance of Long-Range-Corrected Density Functionals for Calculating the Absorption Spectra of Silver Clusters. *J. Phys. Chem. A* **2013**, *117*, 4267–4278.

(47) Rabilloud, F. Description of Plasmon-Like Band in Silver Clusters: The Importance of the Long-Range Hartree-Fock Exchange in Time-Dependent Density-Functional Theory Simulations. *J. Chem. Phys.* **2014**, *141*, 144302.

(48) Dreuw, A.; Head-Gordon, M. Failure of Time-Dependent Density Functional Theory for Long-Range Charge-Transfer Excited States: The Zincbacteriochlorin-Bacteriochlorin and Bacteriochlorophyll-Spheroidene Complexes. *J. Am. Chem. Soc.* **2004**, *126*, 4007–4016.

(49) Chai, J.-D.; Head-Gordon, M. Systematic Optimization of Long-Range Corrected Hybrid Density Functionals. *J. Chem. Phys.* **2008**, *128*, 084106.

(50) Hay, P. J.; Wadt, W. R. Ab Initio Effective Core Potentials for Molecular Calculations. Potentials for K to Au Including the Outermost Core Orbitals. *J. Chem. Phys.* **1985**, *82*, 299–310.

(51) Chen, M.; Dyer, J. E.; Li, K.; Dixon, D. A. Prediction of Structures and Atomization Energies of Small Silver Clusters, Ag_n, $n < 100$. *J. Phys. Chem. A* **2013**, *117*, 8298–8313.

(52) Durante, N.; Fortunelli, A.; Broyer, M.; Stener, M. Optical Properties of Au Nanoclusters from TD-DFT Calculations. *J. Phys. Chem. C* **2011**, *115*, 6277–6282.

(53) Perdew, J. P. Density-Functional Approximation for the Correlation Energy of the Inhomogeneous Electron Gas. *Phys. Rev. B* **1986**, *33*, 8822–8824.

(54) Becke, A. D. Density-Functional Exchange-Energy Approximation With Correct Asymptotic Behavior. *Phys. Rev. A* **1988**, *38*, 3098–3100.

(55) van Leeuwen, R.; Baerends, E. J. Exchange-correlation potential with correct asymptotic behavior. *Phys. Rev. A* **1994**, *49*, 2421–2431.

(56) te Velde, G.; Bickelhaupt, F.; Baerends, E.; Guerra, C. F.; van Gisbergen, S.; an T. Ziegler, J. S. Chemistry with ADF. *J. Comput. Chem.* **2001**, *22*, 931–967.

(57) Frisch, M. J.; Trucks, G. W.; Schlegel, H. B.; Scuseria, G. E.; Robb, M. A.; Cheeseman, J. R.; Scalmani, G.; Barone, V.; Petersson, G. A.; Nakatsuji, H. et al. Gaussian 09 Revision D.01. 2009; Gaussian Inc. Wallingford CT.

(58) Allouche, A.-R. Gabedit A Graphical User Interface for Computational Chemistry Softwares. *J. Comput. Chem.* **2011**, *32*, 174–182.

(59) Schira, R.; Rabilloud, F. Effects of Rare-Gas Matrices on the Optical Response of Silver Nanoclusters. *J. Phys. Chem. C* **2018**, *122*, 27656–27661.

(60) Yang, X.; Cai, W.; Shao, X. Structural Variation of Silver Clusters From Ag_{13} to Ag_{160}. *J. Phys. Chem. A* **2007**, *111*, 5048–5056.

(61) Harb, M.; Rabilloud, F.; Simon, D. Optical Absorption of Silver Clusters: A Study of the Effective Potential Core Size. *Chem. Phys. Lett.* **2009**, *476*, 186–190.

(62) Lu, T.; Chen, F. Multiwfn: a Multifunctional Wavefunction Analyser. *J. Comput. Chem.* **2012**, *33*, 580–592.

(63) He, Y.; Zeng, T. First-Principles Study and Model of Dielectric Functions of Silver Nanoparticles. *J. Phys. Chem. C* **2010**, *114*, 18023–18030.

(64) Bernadotte, S.; Evers, F.; Jacob, C. R. Plasmons in Molecules. *J. Phys. Chem. C* **2013**, *117*, 1863–1878.

(65) Bursi, L.; Calzolari, A.; Corni, S.; Molinari, E. Quantifying the Plasmonic Character of Optical Excitations in Nanostructures. *ACS Photonics* **2016**, *3*, 520–525.

This material is available free of charge via the Internet at `http://pubs.acs.org/`.

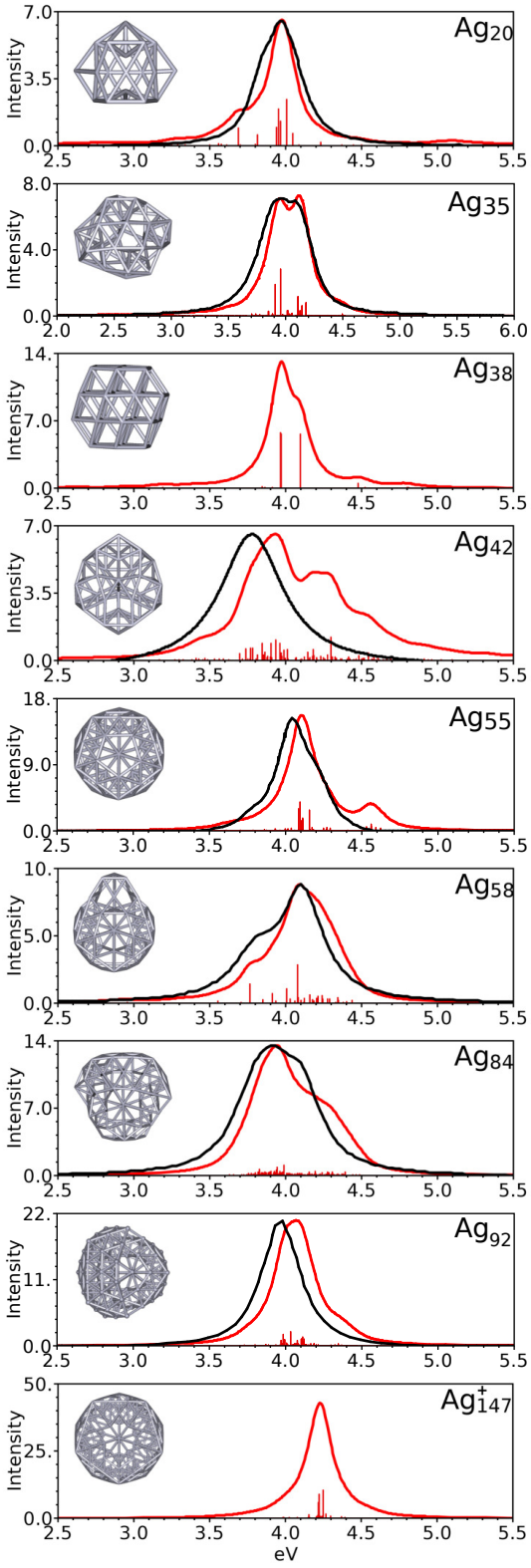

Figure 2: Calculated absorption spectra of silver cluster Ag_n (red lines) together with experimental data (black curves) taken from Ref[23] except the spectrum of Ag_{42} which was measured by surface second harmonic generation spectroscopy on cluters supported on BK7 glass substrate.[30]

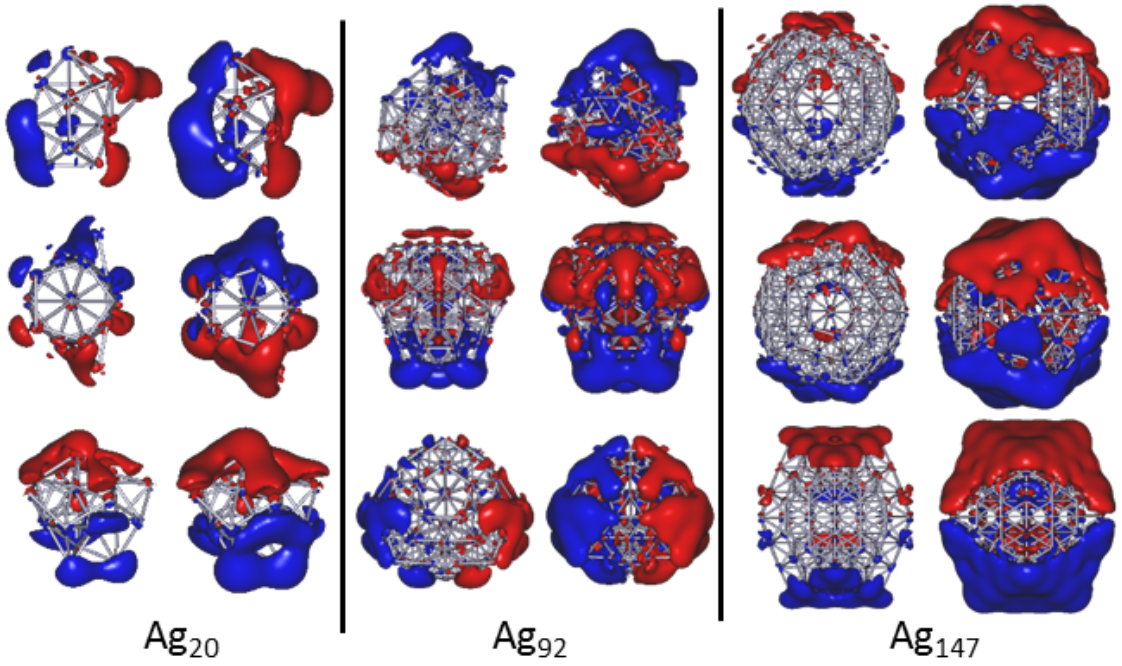

Figure 3: Isosurface plots of the transition density for three main transitions in Ag_{20} (3.98, 4.00, 4.04 eV), Ag_{92} (3.98, 4.03, 4.10 eV) and Ag_{147}^{+} (4.21, 4.22, 4.25 eV). Red and blue surfaces indicate positive and negative isovalues. Isovalue = 0.0006 and 0.0003 for Ag_{20}, 0.0002 and 0.0001 for both Ag_{92} and Ag_{147}^{+}.

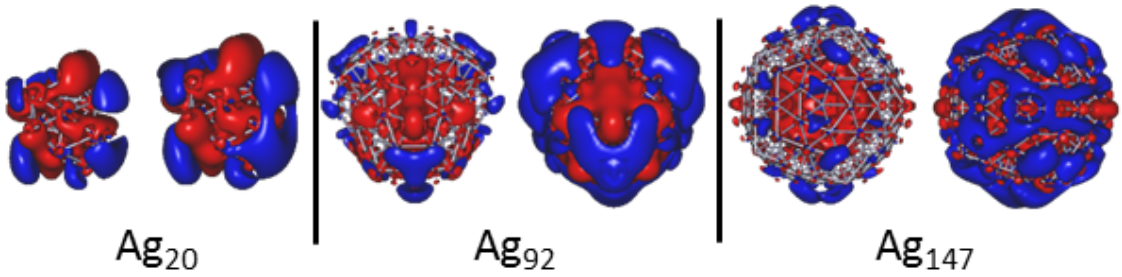

Figure 4: Isosurface plots of the charge density difference between particle and hole (depletion in red, accumulation in blue) for a main transition in Ag_{20} (3.98 eV), Ag_{92} (3.98 eV) and Ag_{147}^{+} (4.21 eV). Isovalue = 0.0001 and 0.00006 for Ag_{20}, 0.00005 and 0.00002 for both Ag_{92} and Ag_{147}^{+}.

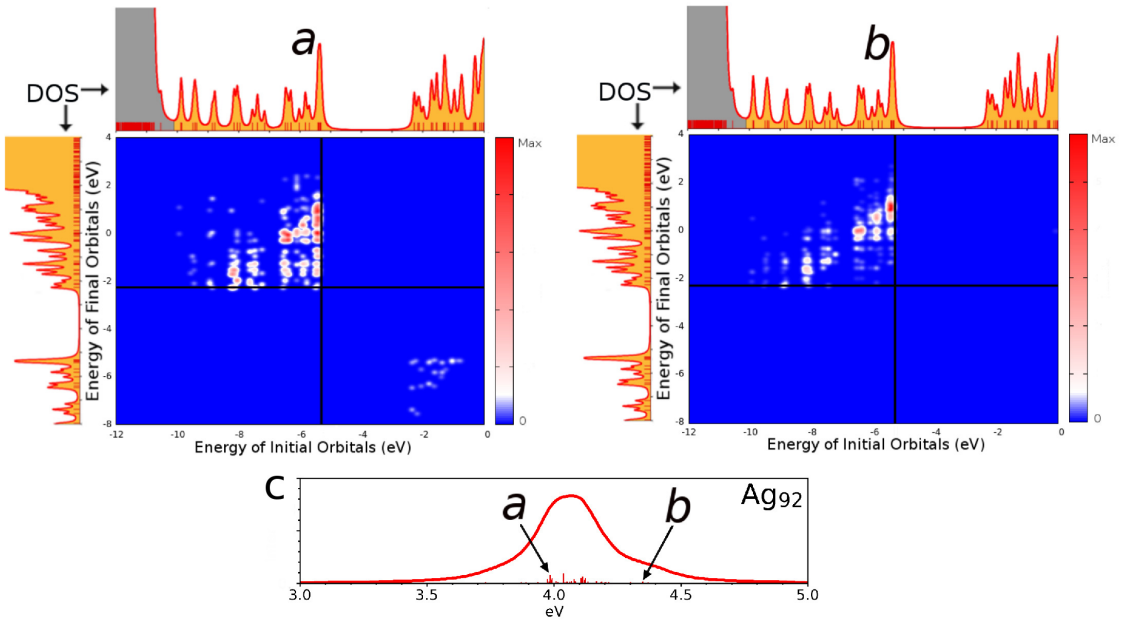

Figure 5: Transition contribution map (TCM) for some excited states of Ag_{92}, together with the Density of states (DOS) where the d and s bands are showed in grey and yellow respectively. Are included transitions with a component $|F_{i,s}| \geq 0.01$. Vertical and horizontal lines represent the energy of the HOMO and LUMO respectively. **a**. TCM for the excited state at 3.98 eV. **b**. TCM for the excited state at 4.35 eV. **c**. Spectrum of Ag_{92}.

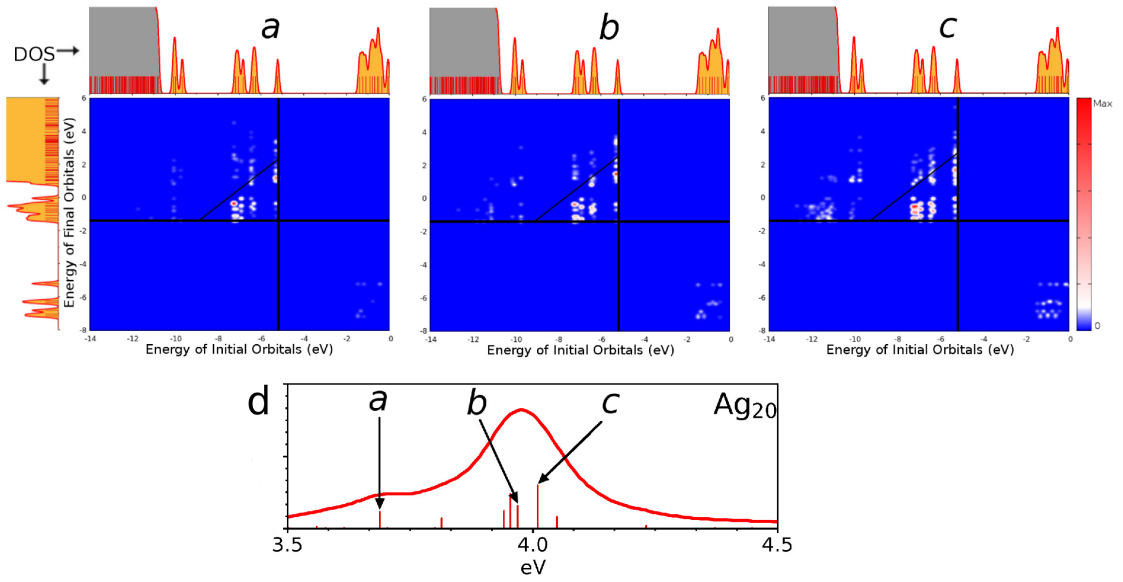

Figure 6: Transition contribution map (TCM) for some excited states of Ag_{20}, together with the Density of states (DOS) where the d and s bands are showed in grey and yellow respectively. Vertical and horizontal lines represent the energies of the HOMO and LUMO respectively. **a**. TCM for the excited state at 3.69 eV. **b**. TCM for the excited state at 3.97 eV. **c**. TCM for the excited state at 4.01 eV. **d**. Spectrum of Ag_{20}.

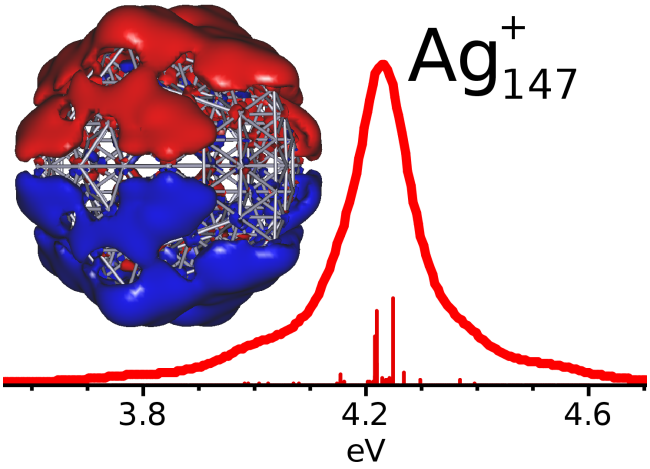

Table of Contents Graphic (TOC)